3D visualization of iron oxidation state in FeO/Fe_3O_4 core-shell nanocubes from electron energy loss tomography.

Pau Torruella,[†] Raúl Arenal,[‡, §] Francisco de la Peña,[,ǁ] Zineb Saghi,[¦] Lluís Yedra,[†] Alberto Eljarrat,[†] Lluís López-Conesa,[†] Marta Estrader,[*,#] Alberto López-Ortega,[⊥] Germán Salazar-Alvarez,[&] Josep Nogués,[Δ, +] Caterina Ducati,[ǁ] Paul A. Midgley,[ǁ] Francesca Peiró,[†] Sonia Estradé[*,†]*

[†]LENS-MIND-IN2UB, Departament d'Electrònica, Institut de Nanociència i Nanotecnologia, Universitat de Barcelona, Martí i Franquès 1, E-08028 Barcelona, Spain.

[‡]Laboratorio de Microscopías Avanzadas (LMA), Instituto de Nanociencia de Aragón (INA), Universidad de Zaragoza, 50018 Zaragoza, Spain.

[§]Fundación ARAID, 50018 Zaragoza, Spain.

[ǁ]Department of Materials Science & Metallurgy, University of Cambridge, 27 Charles Babbage Road, Cambridge, CB3 0FS, UK.

[¦] CEA-LETI, MINATEC, 17 rue des Martyrs, 38054 Grenoble cedex 9, France.

[#]Laboratoire de Physique et Chimie des Nano-objects, 135 Avenue de Rangueil, 31077 Toulouse Cedex 4, France

[&]Department of Materials and Environmental Chemistry, Arrhenius Laboratory, Stockholm University, 10691 Stockholm, Sweden.

[⊥]INSTM and Dipartimento di Chimica "U. Schiff", Università degli Studi di Firenze, Via della Lastruccia 3, Sesto Fiorentino, I-50019 Firenze, Italy

[Δ]Catalan Institute of Nanoscience and Nanotechnology (ICN2), CSIC and The Barcelona Institute of Science and Technology, Campus UAB, Bellaterra, 08193 Barcelona, Spain

[+]ICREA – Institució Catalana de Recerca i Estudis Avançats, Passeig de Lluís Companys, 23, 08010 Barcelona, Spain

Corresponding Authors:

*(S.E.) E-Mail: sestrade@ub.edu

*(M.E.) E-Mail: martaestrader@gmail.com

*(F.D.L.P.) E-Mail: fjd29@cam.ac.uk

This file includes:

Figures S1 to S9, absorption factor estimation and magnetic measurements.

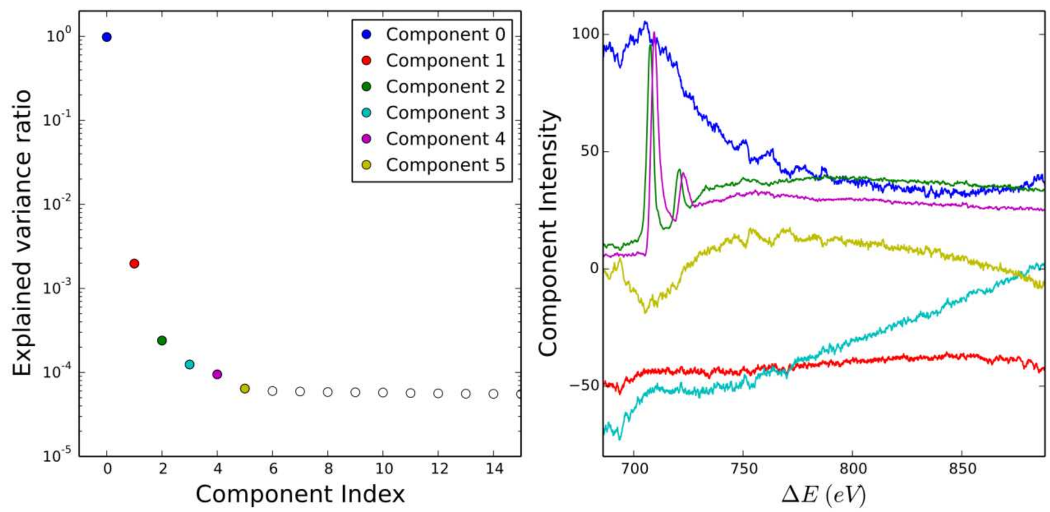

Figure S1. Left panel shows the explained variance ratio of the principal component analysis (PCA) decomposition. The six first components, which are enough to explain the whole data set, are plotted in the right panel. Components 0, 3 and 5 show no remarkable features in the Fe L2,3 ionization energy and seem rather related to the background of the spectra due to their power-law behaviour, while component 1 is almost constant and therefore could be related to the dark noise in the detector.

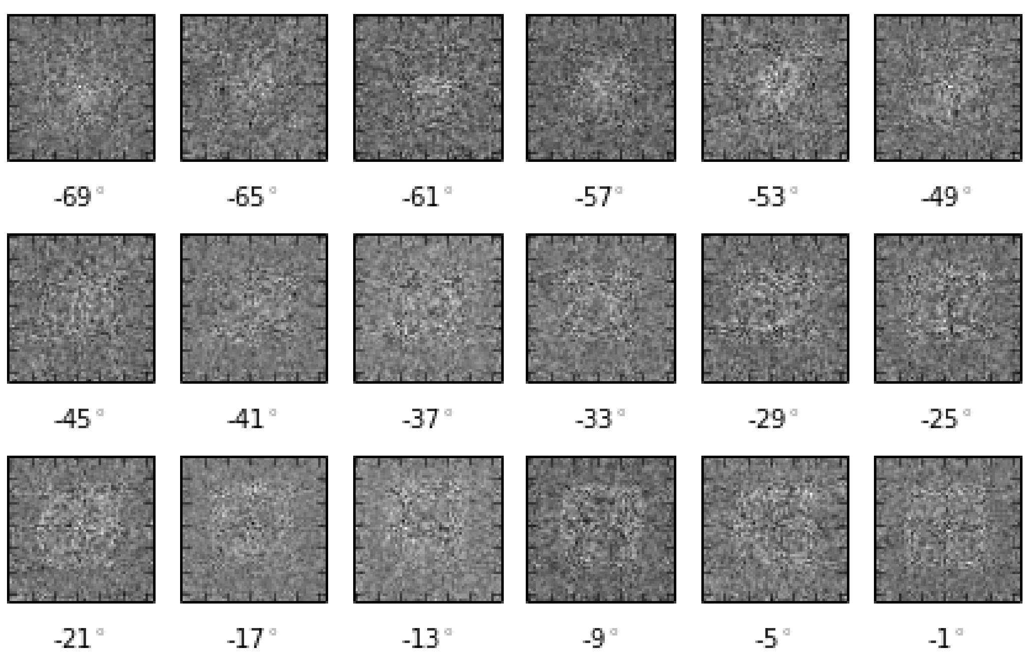

Figure S2. Distribution maps of PCA component 0 for spectrum images at different tilt angles .

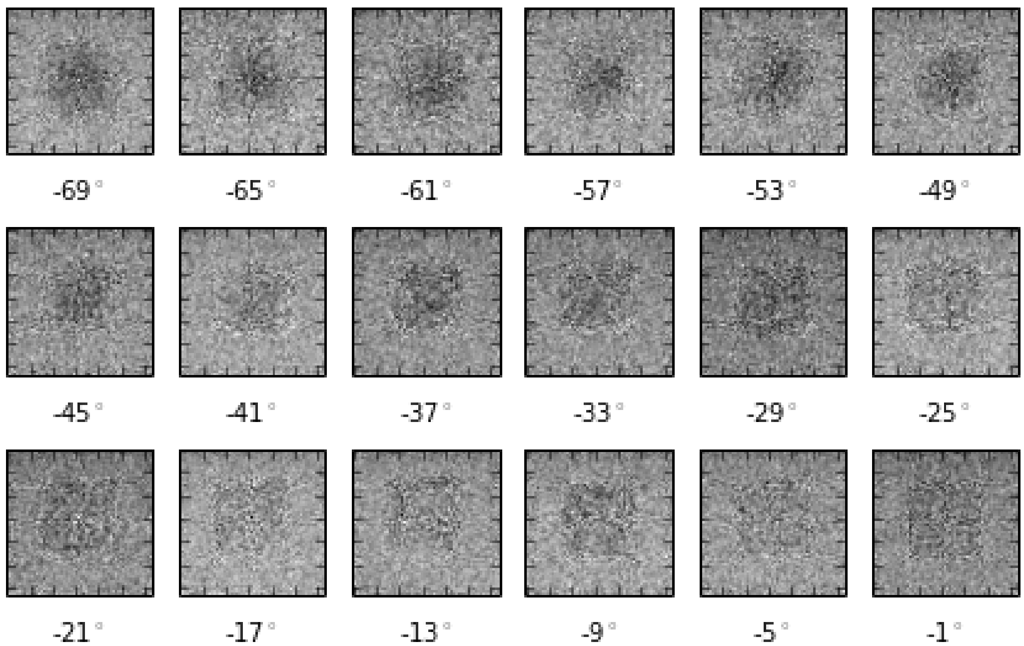

Figure S3. Distribution maps of PCA component 1 for spectrum images at different tilt angles .

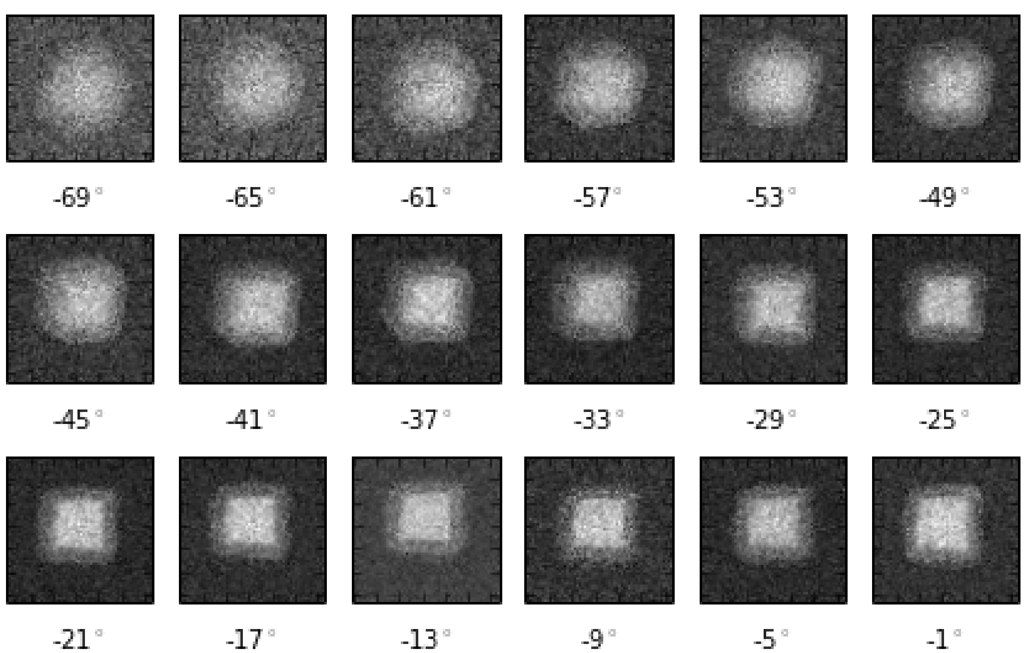

Figure S4. Distribution maps of PCA component 2 for spectrum images at different tilt angles .

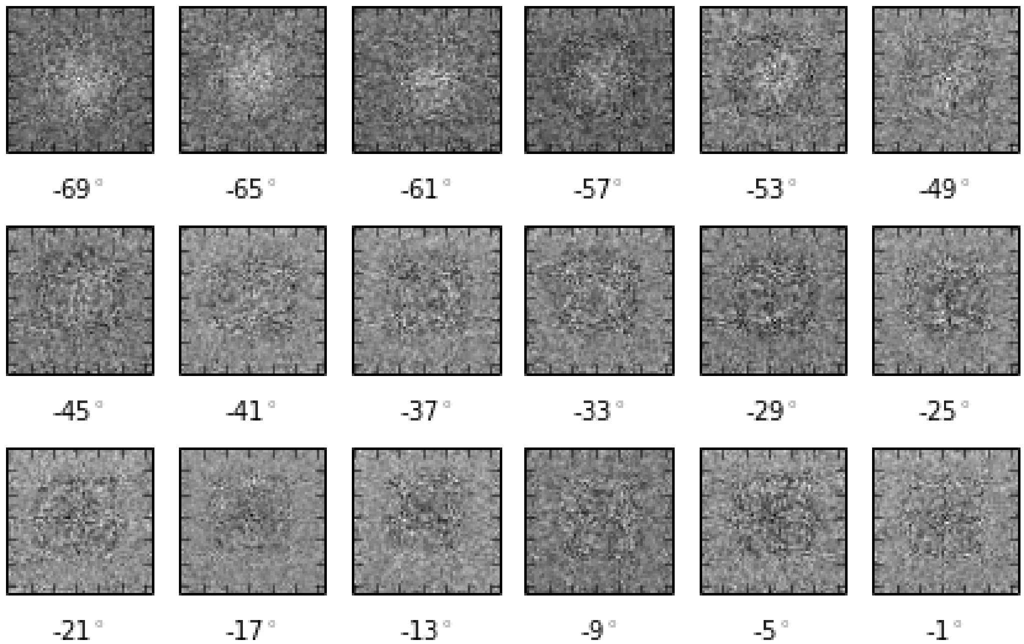

Figure S5. Distribution maps of PCA component 3 for spectrum images at different tilt angles.

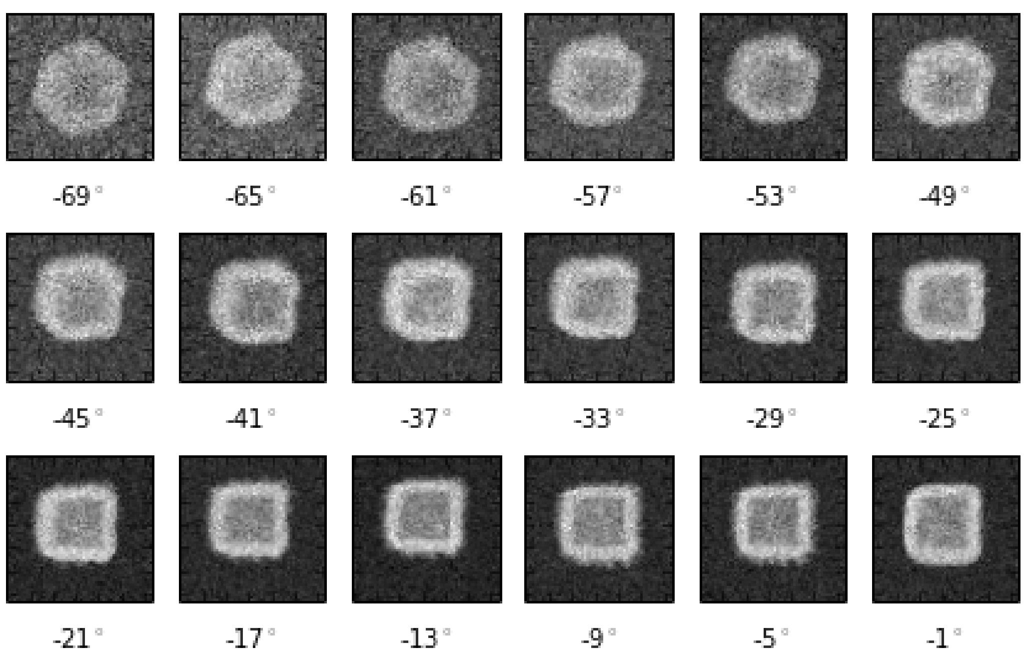

Figure S6. Distribution maps of PCA component 4 for spectrum images at different tilt angles.

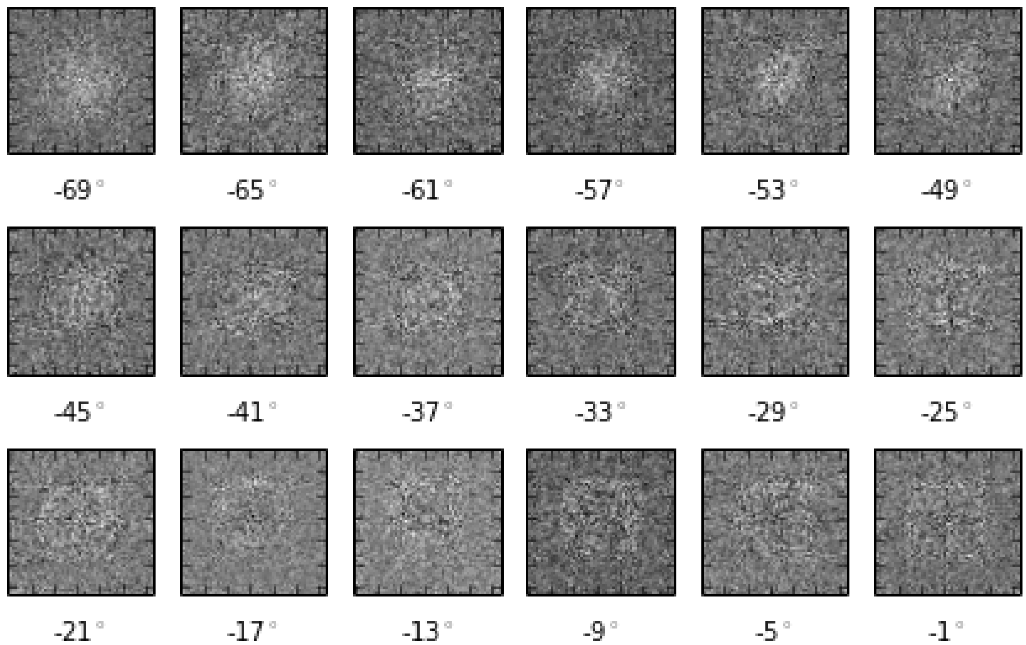

Figure S7. Distribution maps of PCA component 5 for spectrum images at different tilt angles.

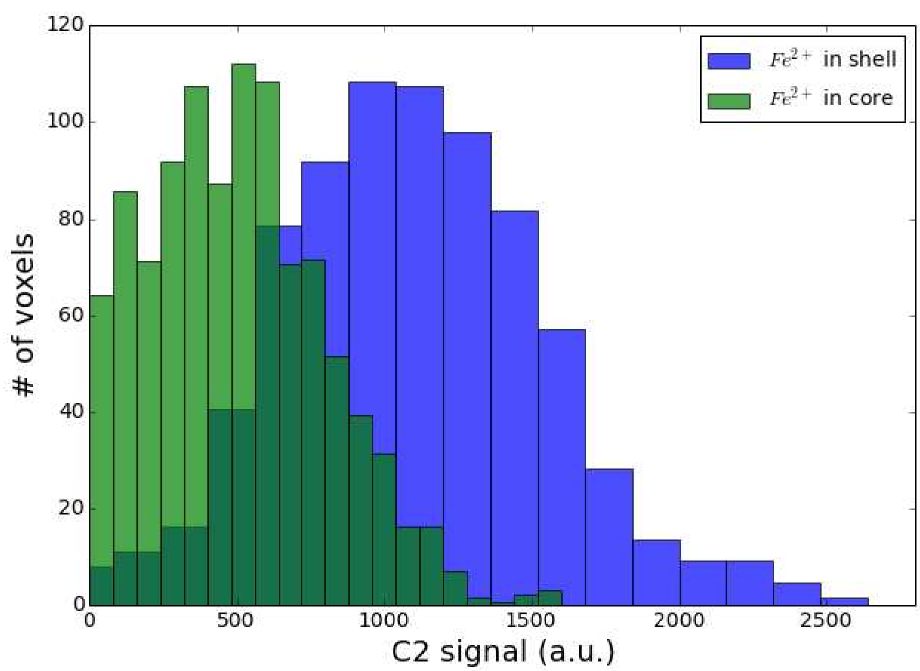

Figure S8. C2 intensity values histogram for voxels in the Fe_3O_4 shell and voxels in the FeO core. Shell distribution is centered at a signal of 500 a.u. while for the core voxels is centered at 1000 a.u., thus giving a ratio of 2, consistent with the composition of both oxides.

Absorption factor estimation

The intensity that ionisation from the Fe $L_{3,2}$ subshells by the electron beam contributes to the EELS spectrum acquired at coordinates x, y and tilt-angle θ at energy E is given by:

$$(1) \qquad I_{FeL_{3,2}}(x, y, \theta, E) = N_{Fe}^{(x,y,\theta)} e^{-\left(\frac{t_{particle}(x,y,\theta)}{\lambda_{particle}} + \frac{t_{substrate}(\theta)}{\lambda_{substrate}}\right)} \sigma_{Fe\,L_{3,2}}(E)$$

where $N_{Fe}^{(x,y,\theta)}$ is the projected iron amount, $\sigma_{Fe\,L_{3,2}}(E)$ is the cross section for ionisation from the Fe $L_{3,2}$ subshells, $t_{particle}$ and $t_{substrate}$ are the thickness of the particle and the substrate respectively and $\lambda_{particle}$ and $\lambda_{substrate}$ their mean free paths. Here we are neglecting plural scattering and the small mean free path difference between Fe_3O_4 and FeO. Also we assume that the substrate is perfectly flat.

We estimate $t_{particle}(x, y, \theta)$ and $t_{substrate}(\theta)$ from the high-angle angular dark field images by segmenting the images by thresholding. From Eq. (1), the intensity of the Fe 3+ and Fe 2+ EELS maps that we have obtained by independent component analysis are given by:

$$(2) \qquad I_{Fe^{2+,3+}}^{(x,y,\theta)} = k_1 N_{Fe^{2+,3+}}(x, y, 0) e^{-\left(k_2 t_{particle}(x,y,\theta) + k_3 t_{substrate}(\theta)\right)}$$

where k 1 , k 2 and k 3 are constants. Summing over x and y and rearranging:

$$(3) \qquad \sum_{(x,y)} N_{Fe^{2+,3+}}(x, y) = k^{-1} \sum_{(x,y)} I_{Fe^{2+,3+}}(x, y, \theta)\, e^{k_2 t_{particle}(x,y,\theta) + k_3 t_{substrate}(\theta)}$$

Notice that we have used $\sum_{(x,y)} N_{Fe^{2+,3+}}(x, y) = \sum_{(x,y)} I_{Fe^{2+,3+}}(x, y, \theta)$ which follows from the fact that the whole particle is contained in the analysed volume. The only unknowns in this equation are k 1 , k 2 and k 3 . k 1 is irrelevant for our purposes. We use Eq. (3) to estimate k_2 and k_3 numerically.

Magnetic Measurements

Magnetic measurements were carried out in a superconducting quantum interference device (SQUID) magnetometer with a maxim field of 70 kOe. The zero field cool magnetization measurements were carried out in 10 Oe with increasing temperature from 10 K after cooling the sample in zero field form the 300 K remanent state. The field cooled hysteresis loop was measured (up to 70 kOe) at 10 K after cooling the sample in H_{FC} = 70 kOe from room temperature.

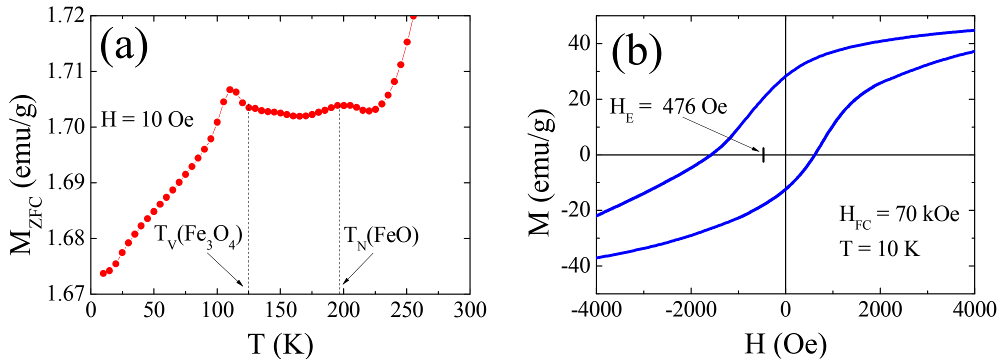

Figure S9. (a) Temperature dependence of the zero field cooled magnetization, M_{ZFC}, of the FeO/Fe_3O_4 nanoparticles measured at H = 10 Oe. The bulk transition temperatures of the Fe_3O_4 Verwey transition, T_V, and the FeO Néel transition, T_N, are shown in the figure. (b) Enlarged hysteresis loop at 10 K after field cooling in H_{FC} = 70 kOe. The loop shift, H_E, is highlighted in the figure.

As can be seen in Fig. 9a, the zero field cooled magnetization, M_{ZFC}, exhibits two clear features at T ~ 110 K and at T ~ 200 K. The low temperature transition can be identified with the Verwey transition, T_V, typical of Fe_3O_4. Since Fe_3O_4 is the only iron oxide featuring this transition, it confirms the presence of Fe_3O_4 in the nanoparticles as revealed by EELS-tomography. Moreover, the rather sharp T_V indicates that the Fe_3O_4 must be rather well structured. On the other hand the high temperature transition can be assigned to the antiferromagnetic Néel trantistion, T_N, of FeO. Since no other iron oxide exhibits any transition in this temperature range, we can safely identify the second counterpart as FeO, in concordance with the EELS-tomography results. Finally, the low temperature hysteresis loop measured after field cooling from room temperature (Fig. 9b) shows a clear loop shift in the field axis, which is typical for ferrimagnetic (FiM) (Fe_3O_4) – antiferromagnetic (AFM) (FeO) exchange coupling, i.e., exchange bias [1]. In fact, the rather large exchange bias shift likely indicates the presence of a well determined interface between the FiM and AFM phases, as observed in Figs. 2-4.

[1] Nogués, J.; Sort, J.; Langlais, V.; Skumryev, V.; Suriñach, S.; Muñoz, J. S.; Baró, M. D. *Phys. Rep.* **2005**, *422*, 65–117.